Experimental Investigation of Hydrodynamic Response of an Ocean Uranium Extraction Machine attached to a Floating Wind Turbine

Maha N. Haji, Jocelyn M. Kluger, Justin W. Carrus, Themistoklis P. Sapsis, and Alexander H. Slocum
Department of Mechanical Engineering, Massachusetts Institute of Technology
Cambridge, MA, USA

ABSTRACT

With conventional sources of uranium forecasted to be depleted within a century, developing methods to cost-effectively harvest uranium from seawater, which is estimated to contain 1000 times more uranium than on land, are crucial to the continued viability of nuclear power generation. Studies have shown that coupling a uranium harvester system with an existing offshore structure, such as a floating wind turbine (FWT), could greatly reduce the cost of harvesting uranium from seawater as it eliminates the need for dedicated moorings and increases the overall energy-gathering ability of the offshore wind farm. This paper explores the hydrodynamic effects of adding a uranium harvester to an offshore floating wind turbine. The experimentally determined hydrodynamic responses of two designs of a Symbiotic Machine for Ocean uRanium Extraction (SMORE) are compared with that of an unmodified FWT. Both SMORE designs utilize adsorbent filament that is enclosed in a hard permeable shell to decouple the mechanical and chemical requirements of the device. It was found that both SMORE designs do not significantly shift the resonant peaks of the FWT.

KEY WORDS: Seawater uranium; offshore floating wind turbine; uranium adsorption; design; hydrodynamics; experiment; prototype.

INTRODUCTION

With global conventional terrestrial reserves of uranium (estimated at 7.6 million tonnes) expected to be depleted in a little over a century (OECD, 2016), it is anticipated that future uranium supplies will come from lower quality sites, resulting in higher extraction costs and even greater environmental impact. Fortunately, approximately 4.5 billion tonnes of uranium exist in the world's oceans (Tamada, 2009) in concentrations of about 3 ppb (Oguma et al., 2011). The most promising method of recovering uranium from seawater is using chelating polymers (Kim et al., 2013). In this method, chelating polymers are deployed in seawater and remain submerged until the amount of captured uranium approaches the adsorption capacity. The polymer is then run through an elution bath to strip off uranium and other metal ions. The polymer may be immersed several times in elution baths before it needs to be regenerated by an alkali wash to free its functional groups, allowing for the reuse of the polymer. The output from the elution process undergoes purification and precipitation typical for mined uranium to produce yellowcake.

Initial concepts for offshore systems for the extraction of uranium from seawater utilized an adsorbent that is deployed and moored for extended periods of time, brought back to shore for the elution process, and redeployed afterward. These stand-alone, intermittent operation systems have significant practical and economic deployment challenges (Seko et al., 2003) and to date none of these systems have become economically viable. Specifically, detailed economic analysis by Schneider and Sachde (2013) found that a major cost driver of seawater uranium extraction is the mooring and recovery of the adsorbent. The Symbiotic Machine for Ocean uRanium Extraction (SMORE) described in this paper utilizes the structure of an offshore floating wind turbine (FWT) to provide the mooring and structural support for an autonomous, offshore uranium harvesting platform. SMORE reduces the mooring and deployment costs of seawater uranium production by continuously passing the adsorbent from the ocean through an elution process and then returning the polymer to the ocean. The integration of a uranium harvesting system with a FWT is pursued because the systems can then share structural support and moorings, which reduces their cost compared to standalone systems (Byers et al., 2016).

SMORE is sized to recover 1.2 tonnes of uranium from seawater per year, enough annual fuel for 5-MW worth of nuclear power (Haji and Slocum, 2016) and is designed to work with the National Renewable Energy Laboratory (NREL) 5-MW wind turbine mounted on the OC3-Hywind floating spar (Jonkman et al., 2009; Jonkman, 2010). Thus, about 200 FWTs would also provide enough yellowcake to manufacture fuel for a 1 GW nuclear power plant. It is important to ensure that the incorporation of the uranium harvester to the FWT will not adversely affect the dynamics of the FWT, which could result in reduced power output by the turbine, increased material requirements for the turbine, or changes in the turbine's operation and maintenance. FWT motion complicates rotor aerodynamics and control, which generally decreases FWT efficiency, and increases FWT structural stresses (Sebastian and Lackner, 2013; Tran and Kim, 2015; Jonkman and Matha, 2009; Kluger et al., 2017). This paper exper-

imentally investigates the hydrodynamic responses of full-scale SMORE designs and compares the responses to that of an unmodified NREL 5-MW OC3-Hywind FWT.

THEORY

The hydrodynamics of the FWT are considered in head-on incident waves of amplitude A and frequency ω which result in heave, X_3, and coupled surge, X_1, and pitch, X_5, degrees of freedom taken about the still water line (SWL), as shown in figure 1. The linear equations of motion of the system are given by

$$(\mathbf{M} + \mathbf{A})\ddot{\xi} + \mathbf{B}\dot{\xi} + \mathbf{C}\xi = \mathbf{X}(t), \tag{1}$$

where $\mathbf{M}$ is the mass matrix, $\mathbf{A}$ is the added mass coefficient matrix, $\mathbf{B}$ is the linear damping coefficient matrix, $\mathbf{C}$ is the restoring coefficient matrix, ξ is the platform displacement about the still waterline, and $\mathbf{X}$ is a matrix of the hydrodynamic excitation forces and moments.

Utilizing a linear frequency-domain analysis, the exciting forces and moments due to plane progressive waves will be assumed to be of the form,

$$X_j(t) = \Re\left\{\mathbb{X}_j(\omega)e^{i\omega t}\right\}, \quad \text{for } j = 1, \ldots, 6, \tag{2}$$

where j is the index for each degree of freedom and $\mathbb{X}_j(\omega)$ is a complex quantity. By virtue of linearity, the turbine's response to wave excitation will be of the form,

$$\xi_j(t) = \Re\left\{\Xi_j(\omega)e^{i\omega t}\right\}, \quad \text{for } j = 1, \ldots, 6, \tag{3}$$

where $\Xi_j(\omega)$ is a complex quantity. Combining (1)-(3) yields the following equations of motion in the frequency domain

$$\left[-\omega^2(M_{ij} + A_{ij}(\omega)) + i\omega B_{ij}(\omega) + C_{ij}\right]\Xi_j(\omega) = \mathbb{X}_i(\omega), \tag{4}$$

where Einstein notation is used for the cross-coupling terms in each equation of motion i.

The principal seakeeping quantity from a linear seakeeping analysis of a floating body at zero speed is the Response Amplitude Operator (RAO), defined as

$$RAO_j(\omega) = \left|\frac{\Xi_j(\omega)}{A/R^n}\right|, \tag{5}$$

where R is the radius of the spar structure of the turbine, $n = 0$ for $j = 1, 3, 5$ and $n = 1$ for $j = 2, 4, 6$.

For the case of an arbitrary shape such as an offshore wind turbine, it is common practice to examine the dynamic response numerically. Jonkman (2010) conducted a numerical study of the hydrodynamic response of the NREL 5-MW OC3-Hywind FWT using the WAMIT computer program (Newman and Sclavounos, 1988; Lee and Newman, 2010). This program uses a three-dimensional numerical-panel method in the frequency domain to solve response of the turbine to linear wave forcing due to potential flow. The excitation force and RAOs determined by Jonkman (2010) will be compared to the results of the excitation forces and RAOs found in the experiment detailed in this paper.
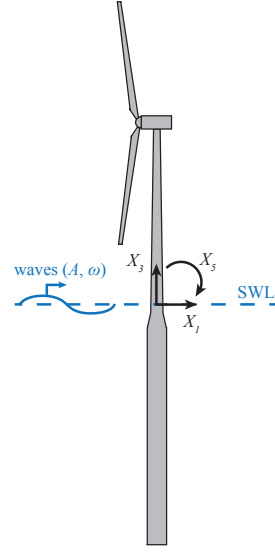

Fig. 1 Floating spar wind turbine, similar to that of the NREL 5-MW wind turbine mounted on the OC3-Hywind spar (Jonkman et al., 2009; Jonkman, 2010) with incident waves of amplitude A and frequency ω. The motions of the turbine are described about the still water line (SWL).

EXPERIMENTAL SETUP

Model scaling

A 1:150 Froude-scaled model of the NREL 5-MW OC3-Hywind FWT and two different versions of SMORE were developed for testing to determine both the wave excitation forces on the structure and the response of each design to the incoming waves. This experiment used a geometric scale, $\lambda = 150$, which is defined to be

$$\lambda = \frac{L_f}{L_m}, \tag{6}$$

where L_f is the full-scale characteristic length and L_m is the model scale characteristic length. Matching the Froude number between the full and model scale using this geometric scale results in different scale ratios for various physical parameters. For instance, while acceleration varies only by a ratio of 1 between the model and full scale, the force scales by a factor of λ^3 (Chakrabarti, 1994).

Models for testing

Two scaled designs of SMORE were developed for testing, in addition to a scale model of the unmodified FWT as reference. The reference FWT was scaled from dimensions detailed by Jonkman, et al. (2009), Jonkman (2010), and Myhr et al. (2014). Some of the key parameters and their full-scale and model values are detailed in table 1. Also included in the table are the actual values used for the reference FWT tested in this study.

The model scale reference FWT was fabricated using aluminum cylinders turned down to the diameters of the upper and lower turbine spar, an aluminum tube for the turbine tower, a circular plate to simulate the rotor damping on the turbine, and a transition region 3D printed from acrylonitrile butadiene styrene. All holes and joints were waterproofed using Permatex Sensor-Safe Blue RTV Silicone Gasket Maker.

Due to fabrication limitations, the model turbine's mass distribution differed slightly from those used by Jonkman (2010). Specifically,

Table 1 Dimensions of the reference FWT (Jonkman, et al. (2009), Jonkman (2010)), the desired 1:150 Froude-scaled model, and the tested model.

| Parameter	Unit	Full-Scale	Desired	Tested
Total draft	m	120	0.800	0.800
Tower height	m	77.6	0.517	0.517
Depth to top of taper below SWL	m	4	0.027	0.027
Depth to bottom of taper below SWL	m	12	0.080	0.080
Diameter above taper	m	6.5	0.043	0.043
Diameter below taper	m	9.4	0.063	0.063
Rotor-hub assembly mass	kg	406,780	0.121	0.104
Tower mass	kg	249,718	0.074	0.075
Total system mass	kg	8,066,00	2.390	2.391
CM location below SWL	m	89.92	0.599	0.592
Water depth	m	320	2.133	1.060

Fig. 2 Design details of SMORE. (a) Hard permeable shell enclosure encapsulating the polymer adsorbent (Haji et al., 2015). (b) A 1/10th physical scale adsorbent ball-chain net as used in SMORE. (c) Side and (d) top views of SMORE which uses rollers to move ball-chain lengths of adsorbent through the water column (Haji and Slocum, 2016).

the tower mass of the FWT reference model used in this study was ~1% heavier than Jonkman (2010). Given that the tower mass of the OC3-Hywind only contributes 3% to the mass of the entire system, this discrepancy in the mass distribution is expected to have a negligible effect. Additionally, the heavier tower mass was compensated by a lighter platform ballast so that the center of mass and moment of inertia of the experimental FWT model matched that used by Jonkman (2010).

The SMORE designs decouple the chemical and mechanical requirements of deploying the adsorbent in the rough ocean environment by using spherical shell enclosures to house the polymeric adsorbent, as shown in figure 2(a) (Haji et al., 2015). These shells are incrementally placed along high strength mooring rope, resembling conventional ball-chain belts. The lengths of shells are connected together using cross-members of high-strength marine grade rope to develop a net-like structure, as shown in figure 2(b). These cross-members decrease the likelihood of tangling between ball-chain lengths and increase the rigidity of the overall component. The ball-chain net is strung between a set of upper and lower rollers to move it through the water column, shown in figures 2(c)-(d) (Haji and Slocum, 2016).

A SMORE design in which an upper platform with the top rollers out of the water, as that described in Haji and Slocum (2016), could have considerable risks due to the wave loads near the surface. Given that wave energy decays exponentially with depth, placing the upper platform significantly beneath the water surface could be one way to mitigate these risks. Therefore, in addition to the unmodified FWT, two SMORE designs were tested. In the first design, SMORE-A, the top set of rollers was placed out of the water at 0.03 m above the SWL (corresponding to 4.5 m in a full-scale design). In the second design, SMORE-B, the top set of rollers was submerged 0.12 m below the SWL (corresponding to 18 m in a full-scale design). Figure 3 shows the three-dimensional models and fabricated designs used for testing.

The adsorbent ball-chain net was modeled using 3 mm diameter (#6 trade size) nickel-plated steel bead chain and the upper and bottom platforms of rollers were 3D printed out of acrylonitrile butadiene styrene.
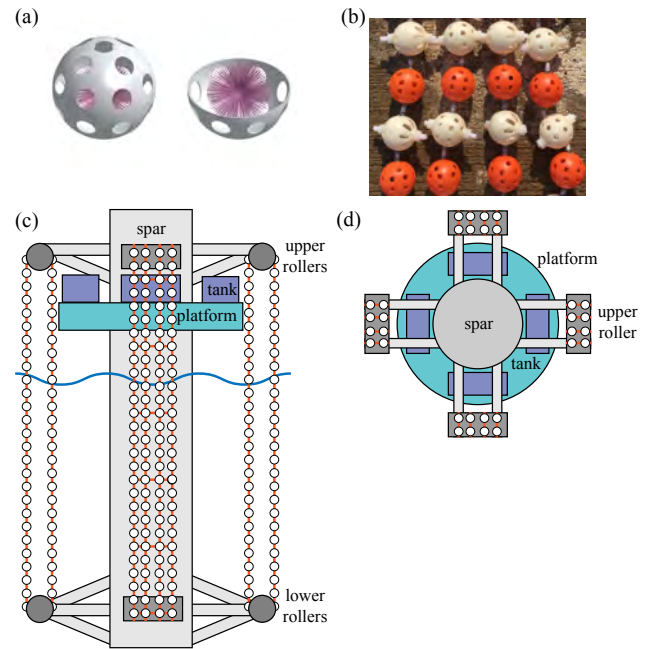
At every five beads, the chains were connected using a thermoplastic adhesive to mimic the increased rigidity that would be provided by rope cross-members of the ball-chain net. Because 3 mm diameter bead-chain was not available in plastic, the bead-chain net added more weight to the model than would be seen in the full-scale version. Therefore, strips of foam were added along the length of the turbine to increase its buoyancy and ensure it had a draft of approximately 0.8 m. The foam strips along the length of the turbine mimicked the additional buoyancy that plastic shells with polymer adsorbents would provide to the overall structure.

The incorporation of the uranium harvesters changed the turbine's parameters of mass, center of gravity and moments of inertia. For instance, SMORE-A (figure 3(b)) added approximately 0.06 kg to the system's weight, an increase of about 2.5% over the unmodified FWT, and shifted the system's center of gravity higher by 0.014 m, or approximately 2.6% higher than that of the unmodified FWT. The wave-tank tests detailed in this paper aim to experimentally investigate how these changes in mass and geometry over the unmodified FWT affect the hydrodynamics of the combined system.

Experimental facilities

The tests described in this paper were conducted in the MIT Tow Tank, which is 30.5 m long, 2.1 m wide, and 1.2 m deep (100 ft long, 8 ft wide, and 4 ft deep). The wave maker at one end is a hydraulically driven vertical paddle with controllable amplitude and frequency that are controlled by LabView.

As shown in figure 4, two wave probes were used to measure the amplitude of the passing waves. One probe was located approximately 9.5 m (31 ft) downstream of the wave maker and another was located at
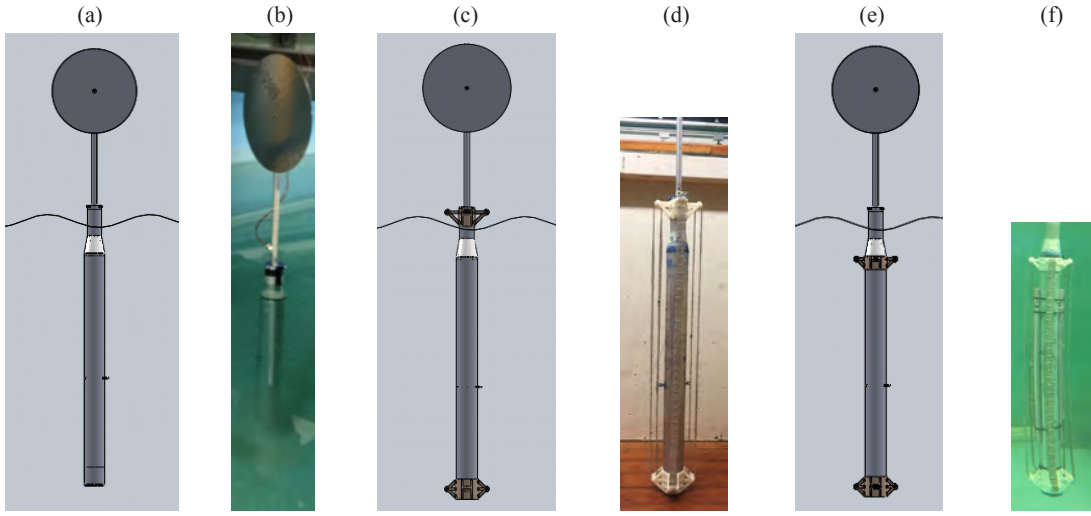
Fig. 3 Three-dimensional solid models and fabricated designs for the reference FWT, (a) and (b), the SMORE design with the upper platform out of the water, (SMORE-A), (c) and (d), and the SMORE design with the upper platform submerged (SMORE-B), (e) and (f).

mid-width in the tank 11.9 m (39.17 ft) downstream of the wave maker, closer to one of the walls of the tank. The models for testing were located about half-way down the length of the tank.
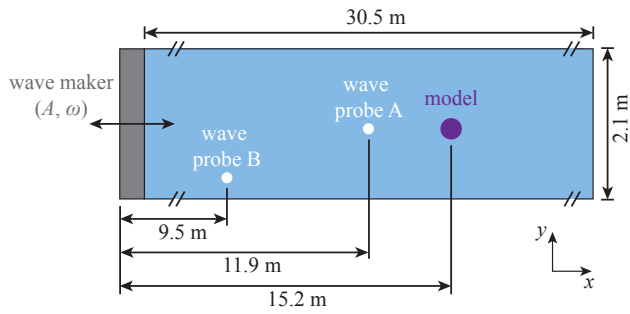

Fig. 4 Schematic of the experimental configuration. The wave maker on the left was excited at an amplitude, A, and frequency ω. Two wave probes (white dots) downstream measured the amplitude incoming to the model (purple) for all tests.

To obtain frequency dependent data for both the wave excitation forces and response amplitude operators, the wave maker was excited at various frequencies and amplitudes for each model test. The wave maker was programmed to excite waves for 20 periods for all tests. Because the wave excitation force varies with frequency, ω, the load cell data were filtered using a Fast-Fourier Transform to obtain the amplitude of the forces at the frequency of interest. Given that the response amplitude operator is also a function of frequency, ω, the acceleration and angular velocity data were also filtered in this way to obtain the amplitude of the response at the frequency of interest.

Excitation Forces

In order to measure the excitation forces on the designs, the models were constrained by a set of three load cells in the configuration shown in figure 5(a). All load cells were SMT Overload Protected S-Type Load Cells. The heave load cell was rated to 1.1 lbf (~ 4.9 N) and the top and bottom surge load cells were rated to 2.2 lbf (~ 9.79 N). Stinger rods measuring 24 mm and 12 mm connected the bottom and top surge, and heave load cell to the turbine tower, respectively. Each load cell
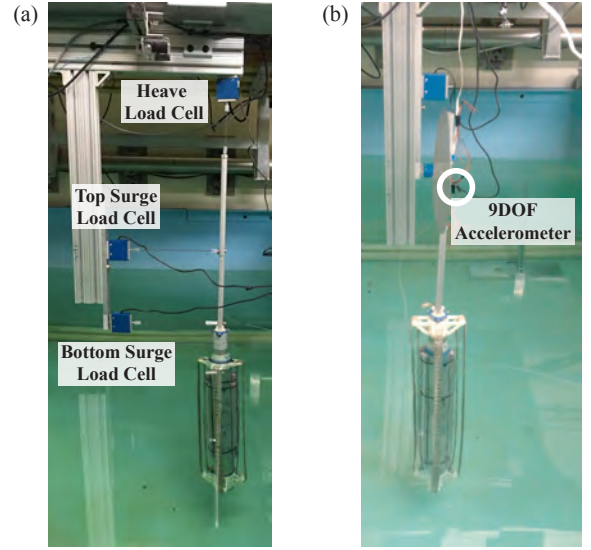

Fig. 5 Experimental setups of the (a) excitation force test and (b) RAO test. In (a) one load cell was used to measure heave and two were used to measure surge. The difference in measurement of the two surge load cells and their distance from the SWL was used to determine the pitch torque. In (b) the 9DOF accelerometer mounted to the tower of the turbine measured heave, surge, and pitch motions.

was connected to a LabView data acquisition unit through a DC powered FUTEK amplifier module to increase the signal readings. The load cells were powered with a stacked dual power supply outputting ~20.7 V for all trials. The bottom surge load cell was approximately 0.057 m above the SWL and the top surge load cell was 0.24 m above the SWL. The surge force was taken to be the sum of the readings of the top and bottom load cells. The resulting pitch torque was determined by

$$X_5 = X_{1,top}z_{top} + X_{1,bottom}z_{bottom}, \tag{7}$$

where $X_{1,top}$ and $X_{1,bottom}$ are the top and bottom surge force load cell readings, respectively, and z_{top} and z_{bottom} are the distances of the load

cells to the SWL, respectively.

Response Amplitude Operators

To determine the response amplitude operators of the models, tests were conducted in which the models were freely floating and an accelerometer mounted to the tower of the turbine measured heave, surge, and pitch motions. The accelerometer was a SparkFun 9 Degree of Freedom Sensor Stick. The accelerometer was configured to measure $\pm$ 2 g in acceleration and $\pm$ 245 deg/s in angular velocity using a Teensy 3.2 USB development board powered through a laptop USB port. The experimental setup is shown in figure 5(b).

Because the accelerometer was mounted above the SWL, the measurements had to be translated by

$$\mathbf{a}^{\mathrm{SWL}} = \mathbf{a}^0 + \boldsymbol{\omega}^{\mathrm{T}} \times \left(\boldsymbol{\omega}^{\mathrm{T}} \times \mathbf{r}^{0,\mathrm{SWL}} \right) + \boldsymbol{\alpha}^{\mathrm{T}} \times \mathbf{r}^{0,\mathrm{SWL}}, \quad (8)$$

where $\mathbf{a}^{\mathrm{SWL}}$ is the acceleration of the turbine at the SWL, $\mathbf{a}^0$ is the acceleration of the turbine measured at the accelerometer, $\boldsymbol{\omega}^{\mathrm{T}}$ is the angular velocity of the turbine as measured by the accelerometer, $\mathbf{r}^{0,\mathrm{SWL}}$ is the position vector from the location of the accelerometer to the SWL, and $\boldsymbol{\alpha}^{\mathrm{T}}$ is the angular acceleration of the turbine, as determined from the accelerometer. Note that because the turbine is assumed to be a rigid body, the angular velocity, $\boldsymbol{\omega}^{\mathrm{T}}$, and angular acceleration, $\boldsymbol{\alpha}^{\mathrm{T}}$ are the same at all points on the body.

RESULTS

The results for the excitation forces and RAOs for all models tested are shown and discussed in this section. All experimentally determined results are compared to the numerical results of the unmodified OC3-Hywind reference FWT (Jonkman, 2010).

Excitation Forces

Figures 6-8 show the full-scale surge excitation force, heave excitation force, and pitch excitation torque, respectively, for the reference FWT, SMORE-A, and SMORE-B. All are normalized per unit wave amplitude.

In the case of the reference FWT, the surge excitation force and pitch excitation torque are slightly larger then the OC3-Hywind FWT numerical results (Jonkman, 2010). This discrepancy is likely due to the fact that the water depth in the wave-tank tests of 1.06 m corresponds to a full-scale water depth of 160 m, whereas the full-scale depth used by Jonkman (2010) was 320 m. According to long wavelength theory,
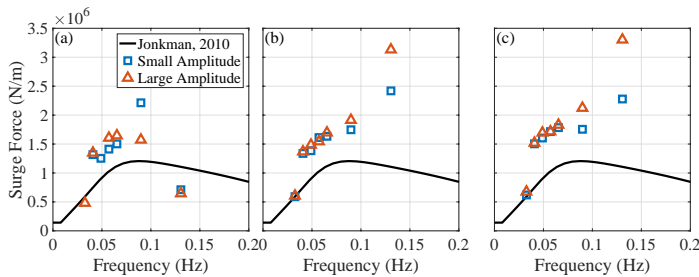

Fig. 6 Full-scale surge excitation force as determined by the load cell tests for small (blue squares) and large (red triangles) amplitude waves as compared to the OC3-Hywind numerical results (Jonkman, 2010)(black line) for the (a) reference FWT, (b) SMORE-A, and (c) SMORE-B.
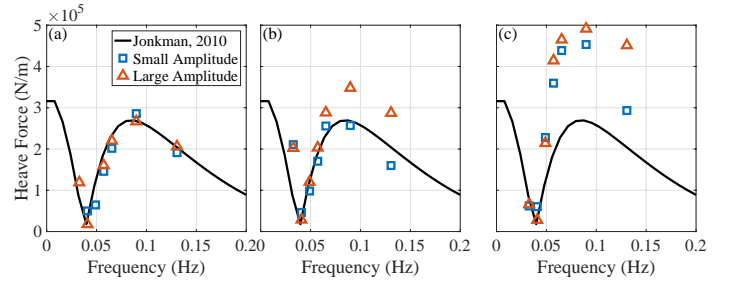

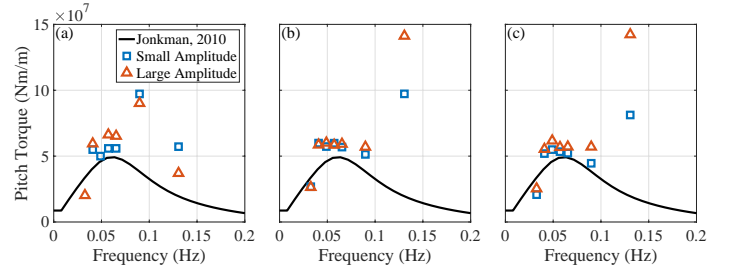Fig. 7 As in figure 6 but for the full-scale heave excitation force.

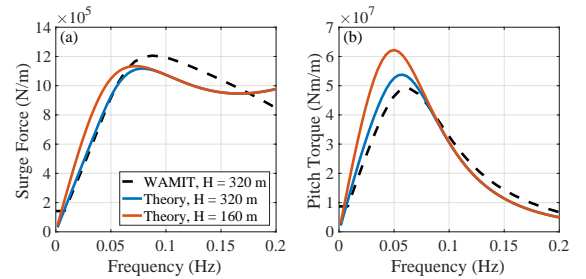Fig. 8 As in figure 6 but for the full-scale pitch excitation torque.

Fig. 9 The full-scale (a) surge excitation force and (b) pitch excitation torque as predicted numerically using WAMIT (black), and by long wavelength theory for water depths of $H = 320$ m (blue) and $H = 160$ m (red).

in the case of the reference FWT the shallower model water depth results in surge excitation forces and pitch excitation torques that are up to ~15% greater than those expected in a perfectly scaled tank test. Furthermore, as shown in figure 9, this magnitude difference only occurs for frequencies less than 0.08 Hz, a trend also observed in the experimental results.

For the case of SMORE-A and SMORE-B, the surge excitation forces (figures 6(b) and 6(c)) and pitch excitation torques (figures 8(b) and 8(c)) have a similar magnitude to the reference FWT tested (figures 6(a) and 8(a)). This suggests that SMORE-A does not significantly affect the FWT surge excitation forces.

As seen in figure 7(a), there is excellent agreement between the heave excitation force for the unmodified FWT as determined from the OC3-Hywind numerical results (Jonkman, 2010) and experimentally measured by the load cells. The experimentally determined heave excitation force for SMORE-A (figure 7(b)) agrees well with the heave excitation force for the unmodified FWT. On the other hand, the heave excitation force of SMORE-B (figure 7(c)) shows an increase in the full-scale heave excitation force compared to the reference FWT (figure 7(a)). This is expected because submerging the upper platform adds a significant amount of heave water plane area excited by waves which results in an increased

heave excitation force.

Response Amplitude Operators

Figures 10-12 show the full-scale surge, heave, and pitch RAOs, respectively, for the reference FWT, SMORE-A, and SMORE-B.

For the unmodified FWT, the experimentally determined surge and pitch RAOs (figures 10(a) and 12(a)) are larger at lower frequencies and smaller at higher frequencies than the OC3-Hywind numerical results (Jonkman, 2010). This is expected as the surge excitation forces and pitch excitation torques (figures 6(a) and 8(a)) were experimentally observed to be larger at frequencies less than 0.08 Hz as compared to the numerical results of Jonkman (2010), a discrepancy that, as seen in figure 9, is likely due to the fact that the numerical results assume a full-scale ocean depth of 320 m, whereas the wave-tank tests correspond to a depth of 160 m.

The surge RAOs for both SMORE-A (figure 10(b)) and SMORE-B (figure 10(c)) show a smaller response at low frequencies and a slightly greater response at high frequencies than the unmodified FWT. This minimal difference in turbine response with the addition of either SMORE design may be due to a change in dampening of the system
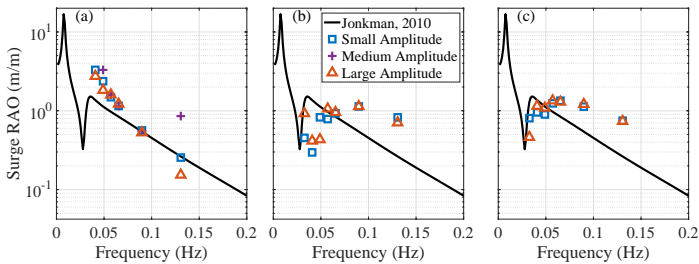

Fig. 10 Full-scale surge RAO as determined by the accelerometer tests for the (a) reference FWT, (b) SMORE-A, and (c) SMORE-B, for small (blue squares), medium (purple crosses) and large (red triangles) amplitude waves as compared to the OC3-Hywind numerical results (Jonkman, 2010) (black line).
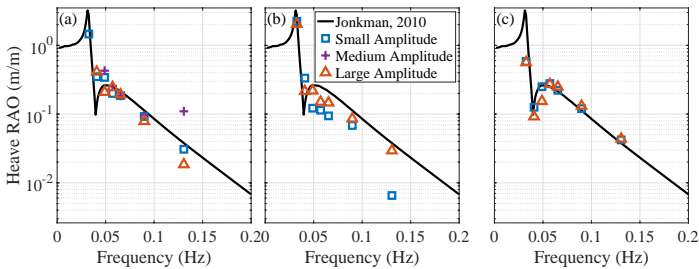

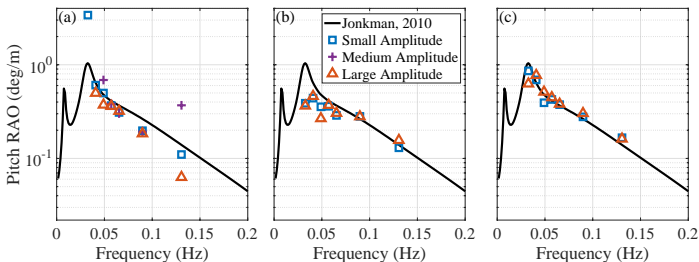Fig. 11 As in figure 10 but for the full-scale heave RAO.

Fig. 12 As in figure 10 but for the full-scale pitch RAO.

caused by the flexible ball-chain nets of SMORE. Moreover, it has been found that the surge motion of the platform decreases when the rotor rotates (Shin, 2011), further suggesting that these changes in the surge motion due to the incorporation of either type of uranium harvester may be minimal.

In the case of the heave RAO, the reference FWT's observed response agrees extremely well with the OC3-Hywind numerical results (Jonkman, 2010) (figure 11(a)). Both SMORE designs show a decrease in the heave response of the system (figures 11(b) and 11(c)) which is likely due to the increased platform mass. Since SMORE-A has the same heave excitation forcing magnitude as the reference FWT (figure 7(a) and (b)), the heave response is smaller than that of the SMORE-B in which the effects of increased force and increased mass on heave motion roughly balance out.

The pitch RAO for SMORE-A (figure 12(b)) shows a decrease in the pitch response as compared to the reference FWT (figure 12(a)), especially near the pitch resonant frequency for the unmodified turbine. This is expected as the additional roller platform near the bottom of the turbine which acts to increase the restoring pitch torque. On the other hand, the pitch RAO for SMORE-B (figure 12(c)) was observed to be about the same as that of the reference FWT. This result is likely due to the fact that in SMORE-B both the upper and lower platforms of the uranium harvester are submerged, with the upper platform imparting a torque that is opposite to the torque of the bottom platform, thereby cancelling out its restoring pitch torque.

SUMMARY AND CONCLUSIONS

The results of the model testing of various SMORE designs indicate that both designs, one in which the upper platform is out of the water (SMORE-A) and another in which it is submerged (SMORE-B), have little effect on the overall hydrodynamics of the wind turbine platform to which the uranium harvester is attached. SMORE-A somewhat reduced the pitch responses of the platform in most frequencies. Some of the discrepancies between the experiment and numerical results may be due to the difference in the full-scale water depth of 320 m used in the numerical studies as compared to 160 m used in the wave-tank tests detailed in this paper.

The results of the model testing of various SMORE designs also indicate that the resonant frequencies of the turbine response are not significantly affected by the incorporation of either of the SMORE systems. This is key because an offshore wind turbine is tuned such that its resonant frequencies are in the range of 0.0077-0.0313 Hz, which are well below the significant ocean wave frequencies.

While this study focused on the linear hydrodynamic response of the SMORE designs, other wave-tank model tests of FWTs have noted the presence of second-order hydrodynamic responses (Goupee et al., 2014), suggesting that the higher-order responses of the SMORE designs should be further investigated. In this study, larger second-order responses were observed in the case of the SMORE designs than the unmodified FWT. Examining the Keulegan-Carpenter (K_C) numbers of the shells shows that they range from ~14-60, suggesting the likelihood of viscous effects such as vortex shedding. Work by Hamlet (2017) also observed a flow-induced oscillation on single ball-chain lengths of SMORE, further suggesting the flexible elements of the ball-chain nets of the uranium harvester may be changing the system's response. Moreover, the ball-chain nets may interact and change the local flow, thereby changing the waves incident on the turbine. While second-order

and viscous hydrodynamics effects are small for the spar buoy FWT (Jonkman, 2010) and its response is largely determined by the turbine's aerodynamics (Roald et al., 2013), further work should investigate how critical these effects may be to the overall SMORE design.

While both SMORE designs may not significantly affect the dynamics of the turbine to which they are attached, other considerations should be taken into account when selecting which SMORE design to deploy. Biofouling, which has been shown to have a detrimental effect on the adsorbent's uranium extract capabilities (Park et al., 2016), could be mitigated by submerging the upper platform as that may reduce light intensity, which is directly correlated to the growth of biological matter, at the adsorbent. The movement of water past the adsorbent's surface may also prevent biofouling as it creates a boundary layer within which it is hard for microorganisms to attach to the adsorbent thereby reducing the initial layer of biofouling. Specifically, research has also shown that there exists critical values of current speeds for different species of marine organisms above which fouling biomass is greatly reduced and in general fouling is not possible at speeds greater than 1.5 m/s (Railkin, 2003). Alternatively, UV light has been shown to have strong antibacterial properties (Lakretz et al., 2010) and thus adding UV LEDs to a point in the adsorbent net's path could also prevent the formation of biofilm and hence reduce biofouling. Moreover, submerging the upper platform beneath the ocean surface could greatly reduce wave loads on the uranium harvester as wave forcing decreases exponentially with depth. On the other hand, designing a chemical system to extract uranium from the adsorbent for SMORE with a submerged upper platform will likely be more difficult than if the platform were above the water. These considerations must be further investigated before designing a symbiotic uranium harvesting system for a large-scale pilot study.

ACKNOWLEDGMENTS

REFERENCES

Byers, M F, et al. (2016). "A Higher Fidelity Cost Analysis of Wind and Uranium from Seawater Acquisition symBiotic Infrastructure,"*Trans. ANS*,115.

Chakrabarti, S K (1994). *Offshore Structure Modeling*, World Scientific, Singapore, SGP.

Goupee, A J, et al. (2014). "Experimental Comparison of Three Floating Wind Turbine Concepts,"*J. Offshore Mech. Arct. Eng.* 136(2), 020906.

Haji, M N, et al. (2015). "Decoupling the functional requirements of an adsorbent for harvesting uranium from seawater through the use of shell enclosure,"*Trans. ANS*, 113.

Haji, M N and Slocum, A H (2016). "Design of a Symbiotic Device to Harvest Uranium from Seawater through the use of Shell Enclosures,"*Trans. ANS*,115.

Hamlet, A (2017). "Uranium Extraction from Seawater: Investigating Hydrodynamic Behavior and Performance of Porous Shells,"*Master's thesis,* Massachusetts Institute of Technology.

Jonkman, J (2010). "Definition of the Floating System for Phase IV of OC3,"*Tech. Rep.*, NREL/TP-500-47535.

Jonkman, J, et al. (2009). "Definition of a 5-MW reference wind turbine for offshore system development,"*Tech. Rep.*, NREL/TP-500-38060.

Jonkman, J and Matha, D (2009). "A Quantitative Comparison of the Responses of Three Floating Platforms,"*Conf. Rep.*, NREL/CP-46726.

Kim, J, et al., (2013). "Recovery of Uranium from Seawater: A Review of Current Status and Future Research Needs,"*Sep. Sci. Technol.*, 48(3), 367-387.

Kluger, J, et al. (2017). "A First-Order Dynamics and Cost Comparison of Wave Energy Converters Combined with Floating Wind Turbines,"in Proc. of *ISOPE 2017*, San Francisco, CA.

Lakretz, A, et al. (2010). "Biofouling control in water by various UVC wavelengths and doses,"*Biofouling*, 26, 257–267.

Lee, C H, and Newman, J (2010). *WAMIT User Manual*, WAMIT, Inc., Chestnut Hill, MA.

Myhr, A, et al. (2014). "Levelised cost of energy for offshore floating wind turbines in a life cycle perspective,"*Renewable Energy*, 66, 714–728.

Newman, J, and Sclavounos P (1988). "The computation of wave loads on large offshore structures,"in Proceedings of *BOSS*.

OECD Nuclear Energy Agency (2016). "Uranium 2016: Resources, Production and Demand,"*Tech. Rep.*, OECD NEA and the IAEA.

Oguma, K, et al.(2011). "Determination of uranium in seawater by flow-injection preconcentration on dodecylamidoxime-impregnated resin and spectrophotometric detection,"*Talanta*, 84(5), 1209-1214.

Park, J, Gill, et al., (2016). "Effect Of Biofouling On The Performance Of Amidoxime-Based Polymeric Uranium Adsorbents,"*Ind. & Eng. Chem. Res.*, 55, 4328–4338.

Railkin, A I (2003). *Marine Biofouling: Colonization Processes and Defenses* CRC Press.

Roald, L, et al., (2013). "The Effect of Second-Order Hydrodynamics on Floating Offshore Wind Turbines,"in Proc. of *DeepWind'2013*, Trondheim, Norway.

Schneider, E and Sachde, D (2013). "The Cost of Recovering Uranium from Seawater by a Braided Polymer Adsorbent System,"*Sci. Glob. Sec.*, 21(2), 134-163.

Sebastian, T and Lackner, M (2013). "Characterization of the unsteady aerodynamics of offshore floating wind turbines,"*Wind Energy*, 16, 339–352.

Seko, N, et al. (2003). "Aquaculture of uranium in seawater by a fabric-adsorbent submerged system, "*Nucl. Technol.*, 144(2), 274–278.

Shin, H (2011). "Model Test of the OC3-Hywind Floating Offshore Wind Turbine, "in Proc. of *ISOPE 2011*, Maui, Hawaii.

Tamada, M (2009). "Current status of technology for collection of uranium from seawater,"*Japan Atomic Energy Agency*.

Tran, T, and Kim, D (2015). "The platform pitching motion of floating offshore wind turbine: a preliminary unsteady aerodynamic analysis,"*J. Wind Eng. Ind. Aero.*, 142, 65–81.